Langmuir

Article

pubs.acs.org/Langmuir

Bimodal Surface Ligand Engineering: The Key to Tunable Nanocomposites

Ying Li,[†,§] Peng Tao,[†,§] Anand Viswanath,[‡] Brian C. Benicewicz,[‡] and Linda S. Schadler*[,†]

[†]Department of Materials Science and Engineering, Rensselaer Polytechnic Institute, Troy, New York 12180, United States

[‡]Department of Chemistry and Biochemistry, University of South Carolina, Columbia, South Carolina 29208, United States

Supporting Information

ABSTRACT: Tuning the dispersion of inorganic nanoparticles within organic matrices is critical to optimizing polymer nanocomposite properties and is intrinsically difficult due to their strong enthalpic incompatibility. Conventional attempts to use polymer brushes to control nanoparticle dispersion are challenged by the need for high graft density to reduce particle core−core attractions and the need for low graft density to reduce the entropic penalty for matrix penetration into the brush. We validated a parametric phase diagram previously reported by Pryamtisyn et al. (Pryamtisyn, V.; Ganesan, V.; Panagiotopoulos, A. Z.; Liu, H.; Kumar, S. K. Modeling the Anisotropic Self-Assembly of Spherical Polymer-Grafted Nanoparticles. *J. Chem. Phys.* **2009**, *131*, 221102) for predicting dispersion of monomodal-polymer-brush-modified nanoparticles in polymer matrices. The theoretical calculation successfully predicted the experimental observation that the monomodal-poly(dimethyl siloxane) (PDMS)-brush-grafted TiO_2 nanoparticles can only be well dispersed within a small molecular weight silicone matrix. We further extended the parametric phase diagram to analyze the dispersion behavior of bimodal-PDMS-brush-grafted particles, which is also in good agreement with experimental results. Utilizing a bimodal grafted polymer brush design, with densely grafted short brushes to shield particle surfaces and sparsely grafted long brushes that favor the entanglement with matrix chains, we dispersed TiO_2 nanoparticles in high molecular weight commercial silicone matrices and successfully prepared thick (about 5 mm) transparent high-refractive-index TiO_2/silicone nanocomposites.

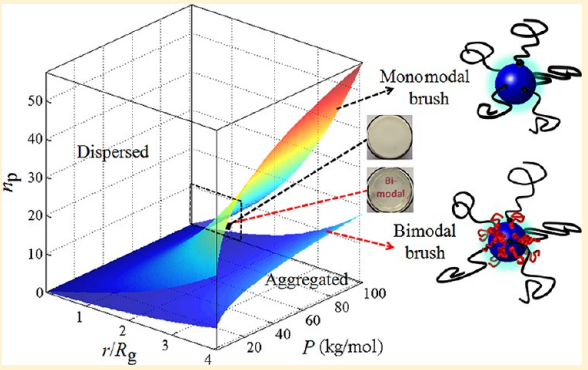

INTRODUCTION

Surface ligand engineering of spherical nanoparticles (NPs) to tailor nanofiller dispersion is one of the grand challenges limiting our ability to harness the potential of nanofilled polymers.[1−3] Optical polymer nanocomposites can uniquely combine the high refractive index (RI) feature of metal oxide NPs and the good processability of polymer matrices. However, the loss of transparency due to scattering from aggregates of NPs severely limited application of polymer nanocomposites as optical filters, LED encapsulants, and advanced optoelectronic packaging materials.[4−6] In order to minimize the scattering loss and prepare transparent optical nanocomposites, a uniform dispersion of nanofillers within a polymer matrix is the key. The basic principle behind surface ligand engineering is the need to shield the surface of the NP and reduce core−core van der Waals (vdW) attraction, while optimizing the wettability of the matrix with the surface ligands.[7−10] Neither small molecule modification nor conventional monomodal (monodisperse) grafted polymer brushes, in general, achieve stable NP dispersion in high molecular weight polymer matrices. Coupling agents such as silanes or surface ligands with carboxylic, amine, or other reactive end groups have shown limited success in improving NP dispersion within solvents or in monomers.[11,12] High optical transparency has only been obtained for very thin films, and the dispersion is not stable when the solvent is removed or the particle volume fraction is high, probably due to insufficient shielding effects of the core−core attraction. In the case of monomodal grafted polymer brushes, shielding the core−core enthalpic attraction requires high surface coverage or a high value of $\sigma\sqrt{N}$ with σ being the brush graft density and N the number of -mers.[13] Thermodynamically stable dispersions of monomodal-polymer-brush-grafted NPs within polymer matrices has been realized using surface-initiated "grafting from" techniques such as atom transfer radical polymerization (ATRP) and reversible addition−fragmentation chain transfer (RAFT) polymerization.[14−16] Although the "grafting from" method has the advantage of controlling the graft density within high-molecular-weight commercial polymer matrices, the entropic penalty is often too high for matrix penetration, and the grafted NPs can suffer from "autophobic dewetting".[17−20] As predicted by the scaling criterion, an entropic attraction between grafted surfaces exists when $\sigma\sqrt{N} > (N/P)^2$ for a polymer matrix with a

Received: September 8, 2012
Revised: October 22, 2012
Published: October 23, 2012

 © 2012 American Chemical Society dx.doi.org/10.1021/la3036192 | *Langmuir* 2013, 29, 1211−1220

degree of polymerization P.[21] One possible explanation for the entropic attraction is that when two brushes come close together, the matrix chains are expelled from the interfacial region and the grafted brushes of two particles interpenetrate and reduce the positive interfacial tension between the grafted and the free polymer chains.[18,21] In order to reduce the entropic penalty and facilitate matrix/brush penetration, either the graft density is decreased at the risk of insufficient core−core screening, or a smaller molecular weight matrix is adopted, which is of little technological importance. This balance between the core−core attraction and entropic repulsion has been modeled by Pryamtisyn et al.,[22] and a qualitative agreement with experimental data has been shown.

In addition to the extensive experimental investigations of monomodal-brush-grafted NP/polymer nanocomposites, powerful simulation tools provide an opportunity to study the influence of bidispersity of grafted chain length on dispersion behavior of grafted NPs prior to experimental studies. Earlier theoretical work has focused on the equilibrium conformation of bimodal brushes in a good solvent.[23−25] It was found that longer brushes were stretched more than the short ones in the region near the interface. The bimodal grafted brush design has been utilized to reduce the entropic surface tension of high-graft-density monomodal polymer brushes and suppress dewetting of thin polymer films on flat substrates.[26,27] When a polymer brush is composed of chemically distinct polymer species, it is defined as a mixed brush,[28] and extensive research has been carried out on their environmental responsiveness to various solvent conditions.[29,30] Very recently, using a self-consistent Polymer Reference Interaction Site Model, Nair et al. reported a similar conformation for the bimodal brush chains grafted on NPs as for the case of flat surfaces in a good solvent.[31] So far, most studies on the bimodal brushes were focused on large particles or flat substrates in solvents with the aid of simulation tools. To the best of our knowledge, the dispersion behavior of bimodal-brush-grafted NPs within polymer matrices and the utilization of these NPs for preparing optical transparent polymer nanocomposites have not been reported.

Owing to important applications as novel encapsulant materials for light-emitting diodes (LEDs) to improve the light-extraction efficiency, silicones filled with high-RI NPs have attracted significant interest.[32] To produce transparent high-RI nanocomposites for common vinyl polymers such as poly(methyl methacrylate), high-RI inorganic NPs are usually grafted with polymer brushes with various surface-initiation "grafting from" polymerization techniques. However, it would be difficult to apply the same approach for silicones, which are produced through condensation reactions between organic silanes. Therefore, here we use a simple "grafting to" approach to graft poly(dimethyl siloxane) (PDMS) brushes onto TiO_2 NP surfaces, which is a convenient route to introduce end-functionalized polymer chains onto NP surfaces.[33,34] We experimentally compared the dispersion behavior of monomodal- and bimodal-polymer-brush-grafted NPs within silicones of different molecular weights. To disperse NPs within high molecular weight matrices, we focus on bimodal-polymer-brush-grafted NPs with a densely grafted short brush providing enthalpic screening for vdW core−core attraction, and a sparsely grafted long brush encouraging wetting by the matrix. With bimodal-PDMS-brush-grafted NPs, bulk (about 5 mm) high-RI transparent TiO_2/silicone nanocomposites were successfully prepared. We further demonstrated that the dispersion behavior of both monomodal- and bimodal-polymer-brush-grafted NPs agrees well with the theoretical predictions from a parametric model. It is anticipated that the good agreement would provide a robust method for quantitatively predicting dispersions of nanofillers, thereby facilitating the control and design of their dispersions within polymer matrices with appropriate surface ligand engineering.

EXPERIMENTAL SECTION

Materials. Titanium(IV) butoxide (97%), oleic acid (90%), and *tert*-butylamine (98%) were purchased from Sigma Aldrich and used for the synthesis of titanium dioxide NPs. Phosphorus(V) oxychloride ($POCl_3$) and triethylamine (Et_3N) were obtained from Sigma Aldrich and used for modification of hydroxyl-terminated PDMS. Monocarbinol terminated PDMS MCR-C12 (M_w = 1000 g/mol), MCR-C18 (M_w = 5000 g/mol), MCR-C22 (M_w = 10 000 g/mol), and silanol-terminated PDMS DMS-S32 (M_w = 36 000 g/mol) were purchased from Gelest and were used as brush polymers. Polysiloxane resin DMS-V05 (M_w = 800 g/mol), DMS-V25 (M_w = 17 200 g/mol), and Sylgard 184 (M_w estimated as 100 000 g/mol) were purchased from Gelest and Dow Corning, respectively, and used as matrix materials for nanocomposite preparation. Methylhydrosiloxane−dimethylsiloxane copolymer (HMS-301) and platinum−divinyltetramethyldisiloxane complex (SIP6831.2) were purchased from Gelest and used as cross-linking agent and catalyst, respectively.

Synthesis of TiO_2 NPs. Spherical TiO_2 NPs were synthesized using a two-phase thermal synthesis approach.[35] In a typical synthesis, 0.4 mL of *tert*-butylamine was dissolved in 10 mL of DI water and the solution was transferred to a 45 mL stainless steel pressure vessel (Parr). Subsequently, titanium(IV) butoxide (1 mL) and oleic acid (OA) (3 mL) were added into 20 mL toluene and homogeneously mixed. The organic mixture was then transferred to the pressure vessel without stirring. The pressure vessel was heated to 220 °C for 5 h and cooled to room temperature. The resulting TiO_2 particles capped with oleic acid were precipitated with ethanol and recovered by centrifugation at 10 000 rpm for 10 min. The white precipitate was dispersed in chloroform and homogeneously distributed. Near monodisperse TiO_2 NPs covered with weakly bonded OA were obtained. The washing procedure with ethanol was then repeated.

Preparation of Polymer-Brush-Grafted TiO_2 NPs. Silicone compatible PDMS brushes were synthesized through direct modification of commercial hydroxyl-terminated PDMS into a phosphate-terminated PDMS. The phosphate headgroup can then replace the weakly bonded capping ligands on the NP surface and the PDMS brushes were grafted to the TiO_2 NP surface.

1. Synthesis of Phosphate-Terminated PDMS. The phosphate-terminated PDMS chains were obtained via a single step modification.[36] In a typical reaction, a tetrahydrofuran (THF) solution of hydroxyl-terminated PDMS was cooled to 0 °C using an ice-water bath under stirring, and Et_3N and $POCl_3$ were added sequentially with a molar ratio of 1:5:5. $POCl_3$ was added dropwise to the stirred solution. The solution was then allowed to warm to ambient temperature as the ice melted. After 2 days, the reaction was terminated by adding DI water and the pH value was adjusted below 2. The modified PDMS chains were extracted with CH_2Cl_2 and filtered over Na_2SO_4. The CH_2Cl_2 solvent was removed using a vacuum rotary evaporator.

2. Grafting PDMS to TiO_2 NP Surfaces. Compared with the weak binding of carboxylic acid, the organo-phosphate bonds have been reported to bind strongly onto metal oxide surfaces.[36,37] The organic phosphate or phosphonate can replace oleic acid and form more robust anchoring on the TiO_2 NP surface. The modified PDMS was added to the transparent TiO_2 NP chloroform solution and refluxed under stirring for 24 h. The grafted NPs in the solution were precipitated using ethanol and then centrifuged under 10,000 rpm for 10 min. The precipitates were then dispersed in chloroform. The precipitation and redispersion were repeated twice to remove residual free polymer chains. Four types of monomodal-PDMS-brush-grafted TiO_2 NPs, labeled according to the molecular weight of the grafted brush (1000, 5000, 10 000, and 36 000 g/mol), TiO_2_1k, TiO_2_5k, TiO_2_10k, and TiO_2_36k, were obtained. As illustrated in Scheme 1, the bimodal-

dx.doi.org/10.1021/la3036192 | Langmuir 2013, 29, 1211−1220

Scheme 1. Preparation of Bimodal-Brush-Grafted NPs[a]

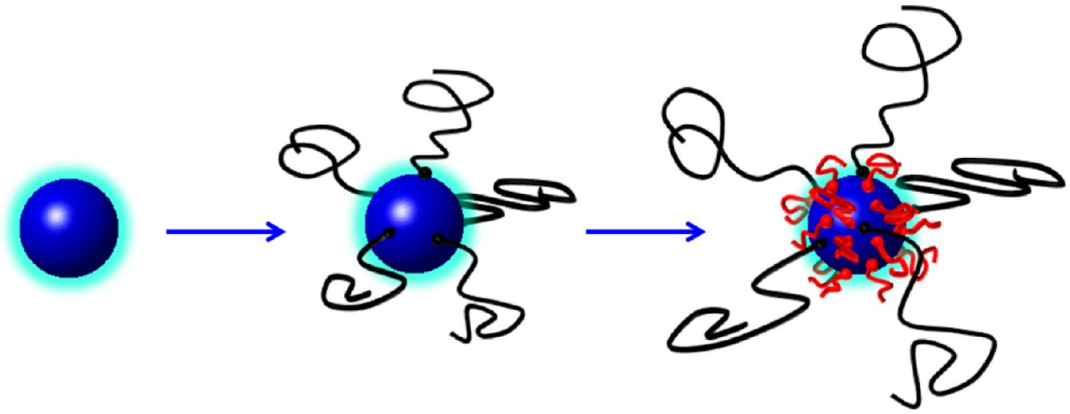

[a]The particle was covered by a surfactant, oleic acid (OA, illustrated as a cyan layer).

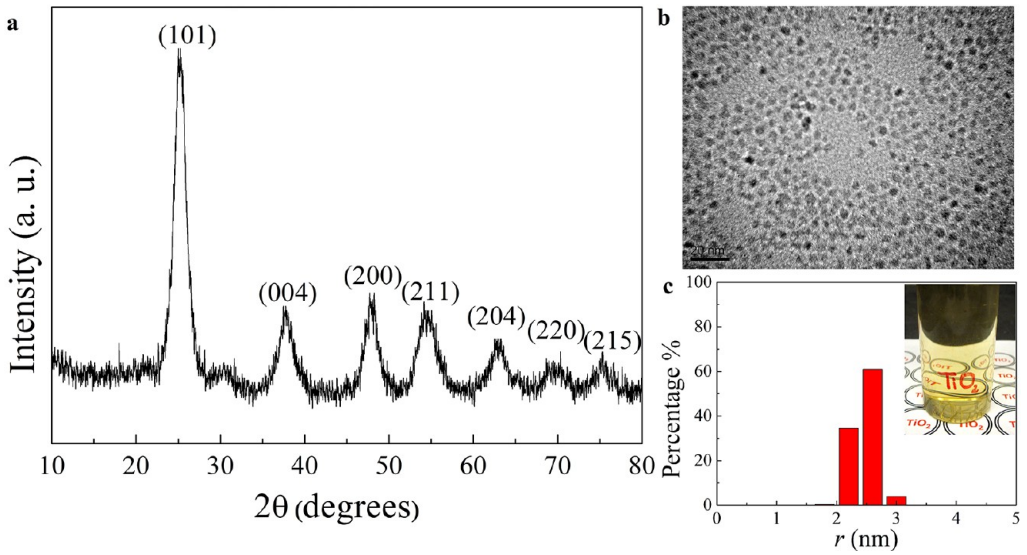

Figure 1. (a) XRD pattern, (b) TEM image, and (c) the size distribution of the as-synthesized TiO_2 NPs. The scale bar is 20 nm. The inset shows a transparent NP dispersion within chloroform.

brush-grafted NP samples were prepared with one additional step after the synthesis of monomodal TiO_2_36k particles. Following the same procedure, TiO_2_36k particles were further reacted with short PDMS chains, and three bimodal samples were obtained, which were labeled TiO_2_36k_1k, TiO_2_36k_5k, and TiO_2_36k_10k according to the molecular weight of the long brush followed by that of the short brush (1000, 5000, and 10 000 g/mol, respectively).

Nanocomposites Preparation. The grafted NPs were dispersed into three silicone matrices, 0.8k, 17.2k, and100k matrices, which are also labeled with their molecular weight (800, 17 200, and 100 000 g/mol, respectively). The grafted TiO_2 NP chloroform solution was added to the neat silicone matrix resin. The mixture was homogeneously stirred and then put under vacuum oven for solvent removal at room temperature. After 3 h, the cross-linking agent (methylhydrosiloxane–dimethylsiloxane copolymer) was added under stirring and the grafted TiO_2 NP/silicone nanocomposite was annealed in vacuum oven at 50 °C to complete solvent removal. Finally, a platinum catalyst (30 ppm) was added to accelerate the curing process. No changes in transparency were observed in the cross-linking step.

Instrumentation and Characterization. X-ray powder diffraction (XRD) patterns were obtained with a Bruker D8 Discover XRD diffractometer using Cu Kα radiation (λ = 1.5405 Å) and operating at an accelerating voltage of 40 kV, in the 2θ range from 10 to 80° (step of 0.01°). Transmission electron microscopy (TEM) images were taken on a JEOL-2010 operating at 200 kV. For silicone nanocomposites, the TEM samples were prepared by microtoming the bulk nanocomposites into 50–70 nm thick slices at −140 °C using an RMC PowerTome cryostat-microtome. Nuclear magnetic resonance (NMR) spectra were recorded on a Varian 500 spectrometer using $CDCl_3$ as the solvent. Thermal gravimetric analysis (TGA) was done on a Perkin-Elmer Series 7 instrument. The NP samples were heated to 800 °C under a N_2 flow at a heating rate of 10 °C/min. The refractive index of the nanocomposites was measured by variable angle spectroscopy ellipsometry (VASE, J.A Woollam Co.) on a spin-coated sample with a thickness in the range of 50–100 nm on a Si wafer. The measured results were fitted with the Cauchy model. Transmittance spectra were obtained with a Perkin-Elmer Lambda 950 spectrophotometer in the range of 300–800 nm. Thin film samples with an average thickness of 50 μm were coated on a glass substrate. In addition, 5 mm thick self-standing nanocomposites were prepared in a glass mold.

RESULTS AND DISCUSSION

Characterization of the Synthesized TiO_2 NPs. The X-ray diffraction pattern and a TEM micrograph of the as-synthesized TiO_2 NPs are shown in Figure 1. All the peaks in the XRD pattern can be assigned to pure anatase phase TiO_2 (JCPDS No: 21-1272). Based on the broadening of the (111) diffraction peak, the crystal size of NPs was estimated to be 5.4 nm. The TEM image shows homogeneously distributed, near monodisperse

dx.doi.org/10.1021/la3036192 | Langmuir 2013, 29, 1211–1220

NPs. The particle size was further characterized with the Image J software by measuring NPs from the TEM image. Figure 1c shows a narrow size distribution, and the average particle size was estimated to be 5 nm in diameter, which agrees well with the calculation from XRD broadening. The as-synthesized TiO_2 NPs were capped with OA and dispersible in nonpolar solvents.

Surface Modification of TiO_2 NPs. To compatibilize the as-synthesized TiO_2 NPs with the silicone matrix, organophosphate terminated PDMS chains were grafted onto NP surfaces via a ligand exchange process. The phosphate-terminated PDMS polymers were prepared through a single step modification of commercial hydroxyl-terminated PDMS with phosphoryl chloride. The successful conversion of phosphate-terminated PDMS can be seen from the ^{31}P NMR spectrum. As shown in Figure 2, the large singlet at 1.57 ppm

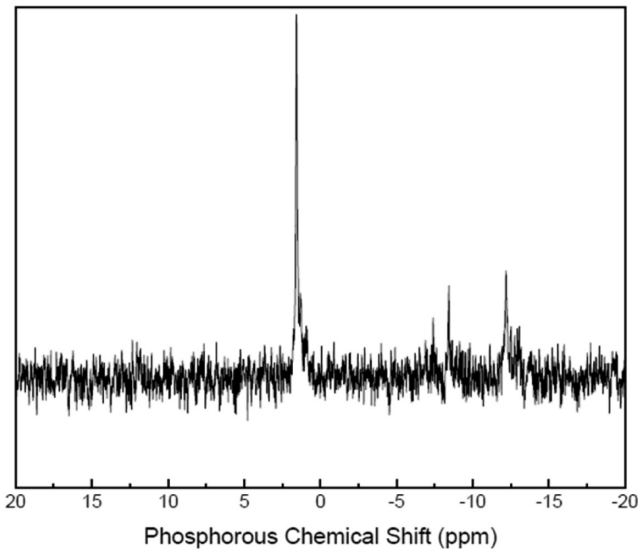

Figure 2. ^{31}P NMR spectrum of phosphate modified PDMS (1000 g/mol).

indicates that the main product is monophosphate PDMS, while smaller peaks at −8 to −12 ppm are diphosphate esters.[36] The phosphor characteristic peaks can be easily identified for the small-molecular-weight PDMS. But the signal becomes too weak to be detected by the spectrometer for the large-molecular-weight PDMS. The phosphate group has stronger binding capability with metal oxide and can partially replace the original synthetic OA.[36]

As shown in Scheme 1, both monomodal and bimodal PDMS chains were grafted onto the surface of TiO_2 NPs. The bimodal-PDMS-grafted NPs were prepared by first attaching the long (36,000 g/mol) PDMS chains followed by grafting of the shorter PDMS chains. The successful grafting of PDMS chains can be seen from the increased weight loss in the TGA curves (Figure S1, Supporting Information). Based on the weight loss due to decomposition of the grafted PDMS chains, the graft density of PDMS was estimated (Table 1).[38] The TGA weight loss due to the grafting of long chains and short chains was used to estimate the graft density. A sum of the two densities is also listed as the effective graft density for the bimodal brush. The graft density of the monomodal brushes decreased from 0.22 to 0.01 chain/nm^2 as the molecular weight increased from 1000 to 36 000 g/mol. This is because the "grafting to" method is a self-limiting process during which the polymer chains must diffuse through the existing grafted polymer chains to reach the reactive sites on the NP surface. The longer the grafted chain, the more pronounced the barrier, for the attachment of subsequent polymer chains. The resulting graft density decreases rapidly with increasing brush chain molecular weight (number of repeating units, N) following an empirical power-law dependence ($\sigma \sim N^{-0.76}$ in our case).[39] With the achieved graft densities, the distance between grafting sites is larger than two times the radius of gyration of grafted PDMS chains. Therefore, they all take a polymer brush conformation on the particle surface.[39] Also, it can be seen that the existence of the initially grafted long chains (36k brush) did not prevent the later grafting of short phosphate-PDMS chains as they have effective graft densities comparable to their monomodal counterparts. The graft density of the shorter chains of the bimodal brush showed a weaker dependence on the chain length ($\sigma \sim N^{-0.38}$).

Table 1. Graft Densities of PDMS-Grafted TiO_2 NPs[a]

grafted NPs	σ_{mono} (ch/nm^2)	σ_{bi} (ch/nm^2)	σ_{eff} (ch/nm^2)
TiO_2_1k	0.22		0.22
TiO_2_5k	0.08		0.08
TiO_2_10k	0.05		0.05
TiO_2_36k	0.01		0.01
TiO_2_36k_1k	0.01	0.08	0.09
TiO_2_36k_5k	0.01	0.05	0.06
TiO_2_36k_10k	0.01	0.03	0.04

[a] σ_{mono} represents the graft densities for monomodal brushes, and σ_{bi} characterizes the graft densities of the subsequent short brushes of TiO_2_36k NP. The sum of σ_{mono} and σ_{bi} is given as effective graft density σ_{eff}.

Dispersion State of Grafted TiO_2 NPs within Silicone Matrices. Considered to be especially critical for optical applications, the transparency of the TiO_2/silicone nanocomposites is largely determined by the NP dispersion state, which was examined both by a simple optical method and with TEM observations. As shown in Figure 3a, all the monomodal-brush-grafted NP filled 17.2k and 100k silicones are completely opaque, implying the formation of agglomerates which scatter light. As the matrix molecular weight is decreased to 800 g/mol, the nanocomposite of TiO_2_36k NP is still opaque, while the TiO_2_5k and TiO_2_10k nanocomposites become translucent and the TiO_2_1k sample is highly transparent. Compared with the monomodal brush systems, Figure 3b shows that the nanocomposites of TiO_2_36k _5k and TiO_2_36k _10k change from completely opaque (within 100k and 17.2k matrices) or translucent (within 0.8k matrix) to totally clear. On the other hand, the 17.2k and 100k silicones filled with TiO_2_36k_1k NPs are still opaque, indicating that there seems to be a certain molecular weight requirement for the inner short brushes in order to obtain good dispersion within the high-molecular-weight matrices.

The dispersion state of grafted NPs within the commercial LED encapsulant silicone matrix (100 000 g/mol) was further subjected to TEM observations as these silicones have better mechanical integrity and are more technologically important. As shown in Figure 4, the TiO_2_36k NPs primarily form spherical agglomerates, while assemblies of TiO_2_5k and TiO_2_10k NPs into stringlike morphologies have been observed. The different aggregation morphologies could be related to the graft density of the grafted PDMS brushes. TiO_2_36k NPs with the lowest graft density tend to form spherical agglomerates driven by the isotropic vdW attraction. With increasing graft density, the

dx.doi.org/10.1021/la3036192 | Langmuir 2013, 29, 1211−1220

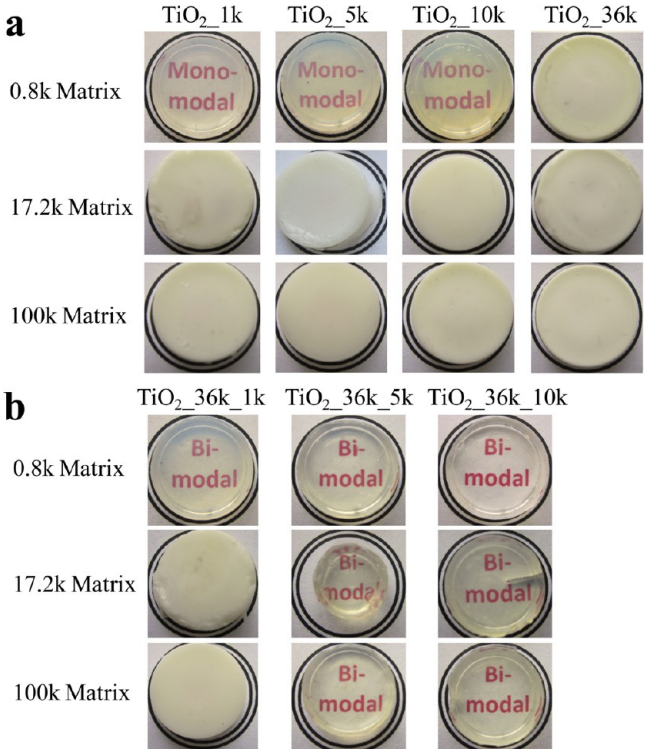

Figure 3. Digital photographs of 5 mm thick silicone nanocomposites filled with 5 wt % (a) monomodal-brush-grafted and (b) bimodal-brush-grafted TiO_2 NPs.

grafted chains have to change their conformation in order to accommodate deformation during contact with adjacent NPs, leading to anisotropic self-assembled structures. Similar anisotropic assembly of polystyrene-grafted silica NPs at low graft density within polystyrene matrices has been reported previously.[40] On the contrary, the TiO_2_36k_10k NPs exhibit a homogeneous dispersion in the 100k matrix, even at higher loading. Given the small size of the TiO_2 NPs, such good dispersion minimizes the transparency loss due to scattering, which explains the transparent nanocomposites obtained using bimodal-PDMS-brush-grafted NPs.

Optical Properties of the Transparent TiO_2/Silicone Nanocomposite. In order to demonstrate the practical application of the bimodal surface ligand engineering approach, we prepared bulk transparent high-RI TiO_2 filled silicones with TiO_2_36k_10k NPs. An increase in RI ($\Delta n \approx 0.06$) was achieved with 20 wt % loading of TiO_2 NPs (Figure 5), which generally follows the rule of mixtures for nanocomposites.[6,33,41] Meanwhile, the thin film samples demonstrated almost the same transparency (around 90%) as pure commercial silicone, except for the strong absorption of ultraviolet light below 350 nm due to the incorporation of UV filtering TiO_2 NPs. Therefore, the TiO_2/silicone nanocomposites can be applied as transparent high-RI and UV-filtering optical coatings. For the transparent 5 mm thick nanocomposites, the decreased transparency in the lower wavelength range (400−500 nm) can be attributed to the absorption of blue light by the yellow colored TiO_2 NPs, as shown by the dispersion in solution (Figure 1). In contrast, the loss of transparency due to scattering was effectively suppressed

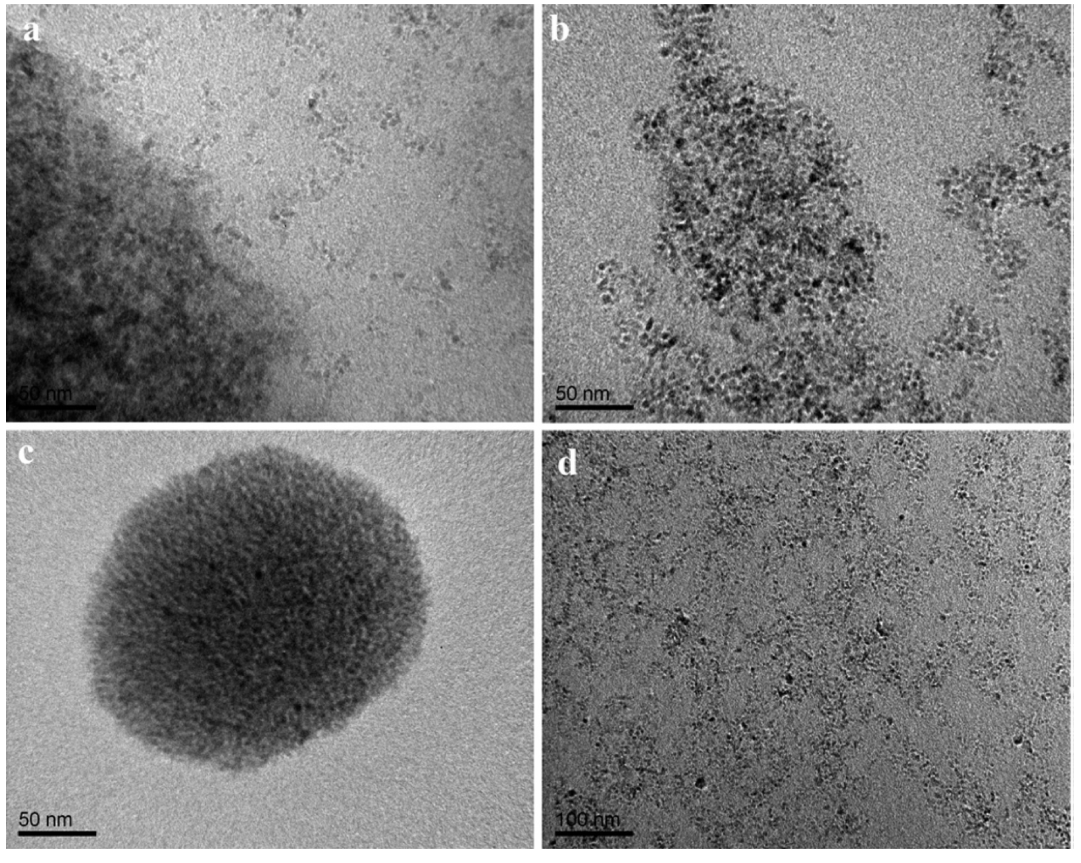

Figure 4. TEM images of silicone nanocomposites of 100k matrix filled with (a) 5 wt % TiO_2_5k NP, (b) 5 wt % TiO_2_10k NP, (c) 5 wt % TiO_2_36k NPs, and (d) 20 wt % bimodal TiO_2_36k_10k NPs.

dx.doi.org/10.1021/la3036192 | *Langmuir* 2013, 29, 1211−1220

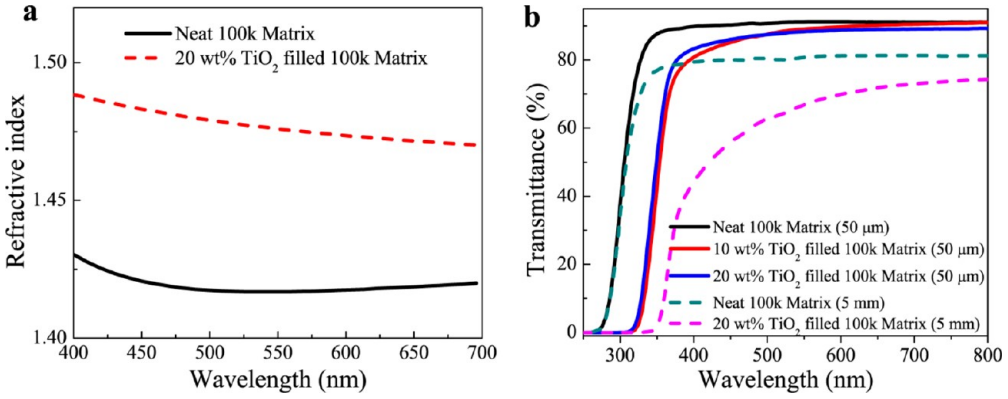

Figure 5. Refractive index dispersion of neat and NP-filled silicones as a function of wavelength (a). UV−vis spectra of neat silicone and bimodal-PDMS-grafted TiO_2/silicone nanocomposites with different thickness and loading (b).

Scheme 2. Geometry Used for Calculation of the van der Waals Core−Core Interaction of Monomodal-Brush-Grafted (a) and Bimodal-Brush-Grafted (b) TiO_2 NPs in the Medium of Silicone

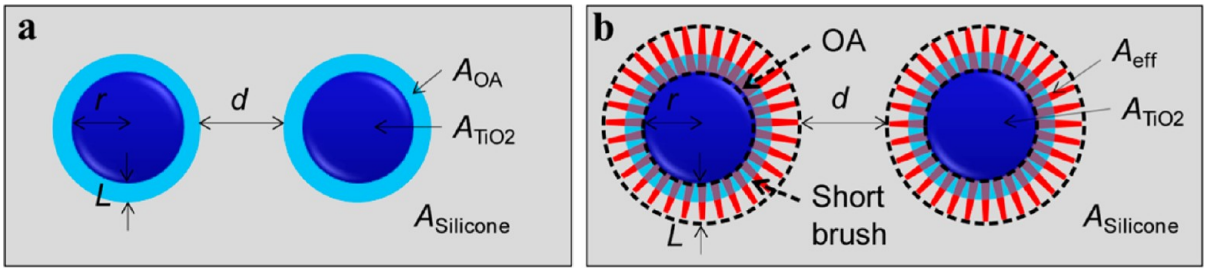

by the good dispersion state as demonstrated by the wavelength independent transparency spectrum from 600 to 800 nm. The transparent high-RI TiO_2/silicone nanocomposites with a thickness up to 1 mm can be used as novel LED encapsulant materials to significantly improve the light-extraction efficiency of LEDs.

Dispersion Phase Diagram. To quantitatively understand the above experimental results and provide a predictive tool across many polymer nanocomposite systems, we adapted the parametric phase diagram model previously developed by Pryamtisyn et al.[22] As indicated by this model, the dispersion state of grafted NPs was determined by the balance between the enthalpic gain and the entropic loss due to the deformation of grafted chains. We reiterate that the phase diagram obtained from this theory was determined by four dimensionless parameters:[22] the energetic gain, χ, resulting from the contact of NPs, the excluded volume parameter $\nu N^2/R_g^3$ where R_g is the radius of gyration of the brush chain and ν is an excluded-volume-interactions-related parameter (which can be approximated as b^3N/P when the brush and matrix chains have same chemistry and b is their Kuhn segment length[22,42]), the total number of grafted chains for each particle n_p, and r/R_g with r being the particle core radius. From previous optical transparency comparison and TEM microstructure analysis, it appears that transparent thick nanocomposites can only be obtained with individually dispersed NPs while all other self-assembled agglomerates lead to opaqueness. Therefore, in our case, the phase diagram is demarcated into just two regions, where "D" stands for dispersed and "A" stands for agglomerated, and the dispersion boundary was obtained by equating the conjunction of enthalpic gain and conformational energy between the well-dispersed state and the stringlike morphology phase in the original model.[22] The Pryamtisyn et al. model[22] provides a clear physical picture about the anisotropic assembly of sparsely grafted spherical nanoparticles. However, to our knowledge, there has been no attempt to utilize this type of model quantitatively for real nanofilled polymer systems.

We first test the model for monomodal-PDMS-brush-grafted NPs. Since it has been suggested that the particle core−core vdW interaction contributes to the tendency for inorganic NPs to aggregate within polymer matrices,[7] the energetic gain, χ, was estimated from the vdW interaction energy of two TiO_2 particle cores capped with OA using eq 1[43] (the geometry is illustrated in Scheme 2).

$$V_{vdW} \simeq -\frac{r}{12}\left[\frac{(\sqrt{A_{silicone}}-\sqrt{A_{OA}})^2}{d} + \frac{(\sqrt{A_{OA}}-\sqrt{A_{TiO_2}})^2}{d+2L} + \frac{(\sqrt{A_{silicone}}-\sqrt{A_{OA}})(\sqrt{A_{OA}}-\sqrt{A_{TiO_2}})}{d+L}\right] \quad (1)$$

Here L is the thickness of the surfactant OA layer, and d refers to the distance between the outer edges of two cores. The three nonretarded Hamaker constants were estimated by eq 2:[44]

$$A_i = \frac{3}{4}k_BT\left(\frac{\varepsilon_i-\varepsilon_{vac}}{\varepsilon_i+\varepsilon_{vac}}\right)^2 + \frac{3h\upsilon_e}{16\sqrt{2}}\frac{(n_i^2-n_{vac}^2)^2}{(n_i^2+n_{vac}^2)^{3/2}} \quad (2)$$

where i could be the silicone matrix, OA, and TiO_2, k_B is the Boltzmann constant, T is the absolute temperature, h is Planck's constant, and υ_e is the main electronic absorption frequency taken to be 3×10^{15} s^{-1} generally.[44] ε and n refer to static

dx.doi.org/10.1021/la3036192 | Langmuir 2013, 29, 1211−1220

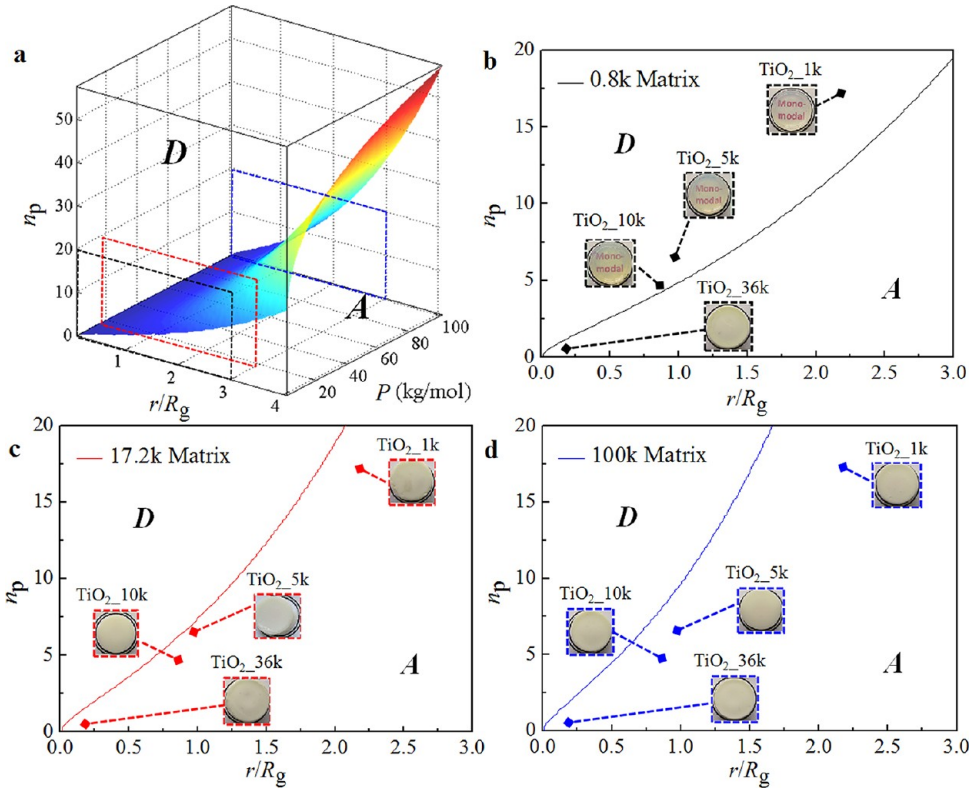

Figure 6. (a) Three-dimensional parametric phase diagram of monomodal-brush-grafted NPs, and its three cross sections are given for (b) 0.8k matrix, (c) 17.2k matrix, and (d) 100k matrix. The inset photos show the corresponding nanocomposites, and the arrows indicate their locations in the phase diagram determined by r/R_g, n_p, and P values.

dielectric constant and refractive index, respectively (Table 1S, Supporting Information).

The calculated vdW attraction between the as-synthesized TiO_2 NP cores ($\sim 10k_BT$) is much larger than the thermal fluctuation at room temperature. The strong opaqueness of the 17.2k and 100k silicones filled with monomodal-PDMS-brush-grafted NPs as well as their anisotropic self-assembly behavior can be attributed to the favorable entropic interaction of the brush with the matrix being insufficient to counterbalance the strong enthalpic attraction.

Based on the calculation (Table 2S, Supporting Information), a three-dimensional parametric phase diagram for the monomodal-PDMS-grafted TiO_2/silicone system was derived (Figure 6). Depending on the ratio of the particle core radius to the radius of gyration of the brush chain (r/R_g), the total number of grafted chains for each particle (n_p), and the degree of polymerization of matrix chains (P) of a specific grafted NP/polymer system, if the system is located within D region in the phase diagram, good dispersion is predicted to be favored. Careful examination of the cross-sectional diagrams reveals that the theoretical predictions are in good agreement with experimental results, in the sense that all the opaque nanocomposite systems are located outside of the D phase. The obvious improvement in dispersion of the TiO_2_1k, TiO_2_5k, and TiO_2_10k NPs within 0.8k silicones can be attributed to the dramatic increase in favorable entropic interaction as the short matrix chains can more easily penetrate into the grafted brush layer. This is confirmed by the expansion of the D phase as the matrix molecular weight decreases. The decreased transparency of 0.8k silicones filled with longer PDMS-grafted NPs implies the importance of high graft density in achieving good dispersion. The monomodal-brush-grafted NPs dispersion results suggest that brushes with comparable chain length to the matrix chain at high enough graft density are required for good dispersion, similar to that observed for flat brushes.[45,46] However, as mentioned above, the graft density decreases rapidly with increasing grafted chain length in the "grafting to" process. Consequently, relatively high graft density was achieved only for the shortest 1k brush ($\sigma \sim 0.22$ ch/nm^2). These dense-short-brush-grafted particles suffered from dewetting within higher molecular weight matrices (17.2k and 100k matrices). As the grafted chain molecular weight increases, the graft densities become too low to counterbalance the strong vdW core−core attraction, leading to the formation of spherical (TiO_2_36k) and anisotropically connected aggregates (TiO_2_10k and TiO_2_5k) in Figure 4. Even if it were possible to increase the brush molecular weight while maintaining a relatively high graft density, the monomodal surface ligand approach would reduce the particle loading that can be achieved because the large molecular weight required for the grafted brush takes up significant volume.

Building on the success of predicting the dispersion of monomodal-brush-modified NPs, we further extend this approach to develop a predictive tool for bimodal surface ligand engineering. To estimate the core−core attraction between bimodal-brush-grafted NPs, the inner short brush together with the OA layer were treated as an effective hybrid layer, as illustrated in Scheme 2b. Accordingly, the Hamaker constant for the hybrid layer, A_{eff}, was estimated from the effective dielectric constant (ε_{eff}) and RI (n_{eff}) as described by eqs 3 and 4 (Table S4, Supporting Information).[47]

$$\log(\varepsilon_{eff}) = \nu_{OA} \log(\varepsilon_{OA}) + \nu_{PDMS} \log(\varepsilon_{PDMS}) \quad (3)$$

dx.doi.org/10.1021/la3036192 | Langmuir 2013, 29, 1211−1220

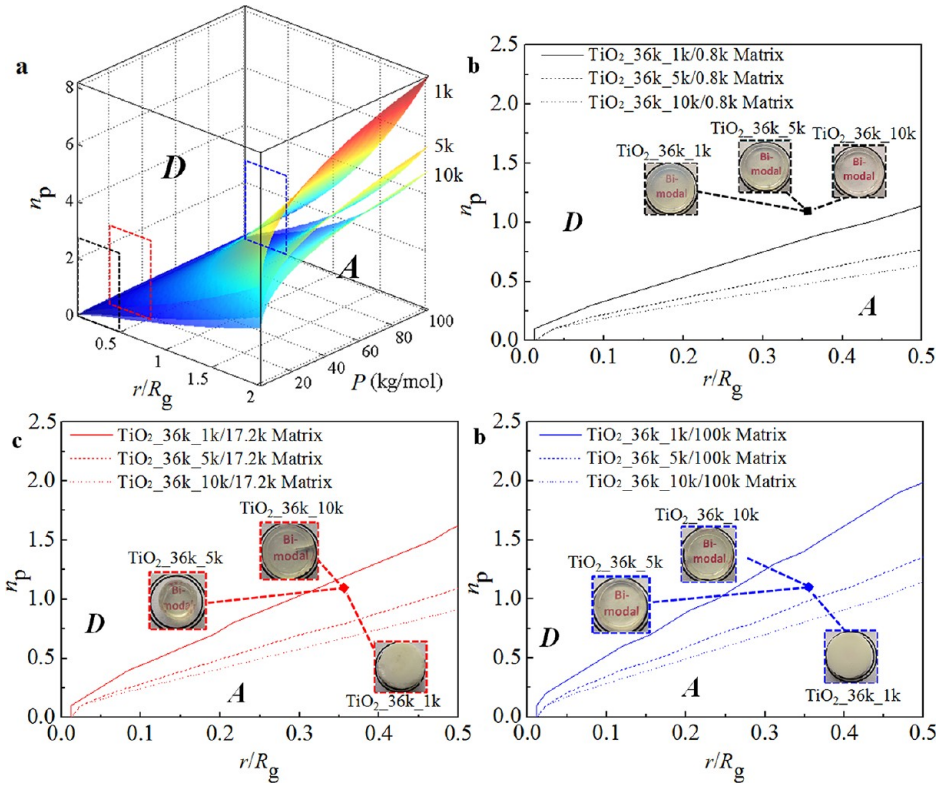

Figure 7. Three dimensional parametric phase diagram showing D phase boundaries of the three types of bimodal-brush-grafted NPs with three different χ_{eff} (a) and its three cross sections are given for 0.8k matrix (b), 17.2k matrix (c), and 100k matrix (d).

$$n_{eff} = v_{OA}n_{OA} + v_{PDMS}n_{PDMS} \quad (4)$$

Then the effective Hamaker constant was used instead of A_{OA} in eq 1 for the calculation of effective enthalpic gain χ_{eff} (the bulk parameters of the corresponding short brush layers are listed in Table S3, Supporting Information). To simplify the calculation, we assume that the inner short brush chains take a random coil conformation with a thickness of the radius of gyration. Given the relatively large molecular weight ratio of the sparsely grafted long brush to the high graft density short brush, it is expected that this would be a reasonable approximation for the short brush. Experimentally, Chevigny et al. examined the correlation between the thickness of a monomodal grafted polystyrene (PS) brush and the dispersion of PS-grafted silica NPs within PS matrices.[48] They found that the grafted layer thickness was very close to the radius of gyration of the grafted chains near the critical point where the dispersion state changed from agglomeration to uniform dispersion. Also, based on their simulation studies of the conformation of bimodal-polymer-grafted NPs within good solvents and an explicit polymer matrix, Nair et al. found that compared with the stretched longer outer brushes the inner brushes tend to be less affected and they behave similar to their monomodal counterparts.[31] The inner short brushes have shown a similar R_g with or without the presence of the polymer matrix.

The good agreement between theoretical predictions and experimental observation of the bimodal-PDMS-brush grafted NPs is shown in Figure 7. As can be seen from the cross-sectional phase diagrams, all the bimodal samples are at the same location in the phase diagram determined by n_p and r/R_g of the same 36k long brush. Thus, whether a nanocomposite is opaque or not depends on its relative location to the D phase boundary. Within the same matrix, the higher the molecular weight of the inner short brush, the larger the D phase region. In other words, an enhanced core−core screening was achieved by increasing the short brush molecular weight as the vdW attraction decays rapidly with interparticle distance. Comparison of the phase diagram in three different matrices shows that the aggregated phase region expands with increasing matrix molecular weight. The initially well-dispersed NPs in the 0.8k matrix are in the aggregated phase region when dispersed within 17.2k and 100k silicone matrices. The bimodal-brush-grafted NPs generally exhibit better dispersion in silicone matrices than their monomodal counterparts, which agrees well with our calculation showing that the D phase expands at the expense of A phase due to decreased χ_{eff}. In addition to the shielding effect of the core−core attraction by the inner short brushes, the penetration of long matrix chains is encouraged by the sparsely grafted long brushes, which favors good dispersion of bimodal-brush-grafted NPs in high molecular weight matrices. The successful suppression of the dewetting phenomenon with 36k grafted long brushes in the 100k silicone matrix is likely also related to the strong curvature effect of the small NPs.[48,49] Such homogeneous dispersion is vital to minimizing the transparency loss from Raleigh scattering and the preparation of transparent nanocomposites.[6] Meanwhile, the persistent opaqueness of 17.2k and 100k silicones filled with TiO_2_36k_1k NPs implies that the 1k inner brush it too short to screen the strong core−core attraction.

Overall, we observed good agreement between experimental results and predictions of the dispersion behavior from the parametric modeling for both monomodal and bimodal systems. For the monomodal brush systems, it is worth noting that, as pointed out by the original model, the parametric phase diagram would work better for intermediate and low graft density NPs, which is appropriate for the graft density achieved with the "grafting to" method here. Second, this model does not include

dx.doi.org/10.1021/la3036192 | Langmuir 2013, 29, 1211−1220

other entropy contributions, such as translational entropy, which can play an important role when the interparticle interaction is not strong. Therefore, this model would be more suitable for our high-RI NPs case. As for the bimodal brush systems, the good agreement further substantiates the original bimodal grafted chain design. Ideally, the phase diagram predicts the dispersion state of the grafted particles at equilibrium states. In our experiment, thermodynamic stability of the dispersion plays a more important role because no changes in dispersion state of the grafted particles within silicones were observed either during the evaporation of the solvent or the final cross-linking step. Finally, it should be mentioned that this parametric quantitative prediction is applicable to other nanocomposite systems filled with grafted nanofillers.[50] We have also successfully predicted the dispersion behavior of PDMS-grafted ZrO_2 NPs in silicones, which will be reported separately.

CONCLUSION

In summary, we modified TiO_2 NPs with monomodal and bimodal PDMS brushes using a simple and versatile "grafting to" approach and studied their dispersion behavior within silicones of different molecular weights. It was found that the monomodal-PDMS-brush-grafted NPs can only be homogeneously dispersed within a smaller-molecular-weight matrix due to the compromise between the achievable graft density and grafted chain length in the "grafting to" process. We have demonstrated the power of bimodal brush modification as a method for dispersing grafted NPs within high-molecular-weight silicones and prepared bulk transparent high-RI TiO_2/silicone nanocomposites. The bimodal polymer brush design has enabled the modification of inorganic NPs and achieved tunable dispersions with the simple "grafting to" method. More importantly, for the first time, we have experimentally validated a parametric phase diagram, and have extended the phase diagram to predict the dispersion for bimodal-polymer-brush-grafted NPs. The quantitative predictive tool opens up the opportunity for advanced polymer nanocomposite design.

ASSOCIATED CONTENT

Supporting Information

Parameters used in theoretical calculations. This material is available free of charge via the Internet at http://pubs.acs.org.

AUTHOR INFORMATION

Corresponding Author

*E-mail: schadl@rpi.edu. Telephone: (518) 276-2022. Fax: (518) 276-8554.

Author Contributions

[§]These authors contributed equally.

Notes

The authors declare no competing financial interest.

ACKNOWLEDGMENTS

This work was supported by the Engineering Research Center Program of the National Science Foundation under Cooperative Agreement EEC-0812056 and by NYSTAR under contracts C080145 and C090145. The authors also acknowledge the financial support by the Nanoscale Science and Engineering Initiative of the National Science Foundation under NSF award number DMR-0642573. The authors thank Xufeng Zhang (Yale University) for his assistance with the theoretical calculations.

REFERENCES

(1) Mackay, M. E.; Tuteja, A.; Duxbury, P. M.; Hawker, C. J.; Van Horn, B.; Guan, Z.; Chen, G.; Krishnan, R. General Strategies for Nanoparticle Dispersion. *Science* **2006**, *311*, 1740−1743.

(2) Vaia, R. A.; Maguire, J. F. Polymer Nanocomposites with Prescribed Morphology: Going Beyond Nanoparticle-Filled Polymers. *Chem. Mater.* **2007**, *19*, 2736−2751.

(3) Kumar, S. K.; Krishnamoorti, R. Nanocomposites: Structure, Phase Behavior, and Properties. *Annu. Rev. Chem. Biomol. Eng.* **2010**, *1*, 37−58.

(4) Yamada, S.; Mouri, E.; Yoshinaga, K. Incorporation of Titanium Dioxide Particles into Polymer Matrix Using Block Copolymer Micelles for Fabrication of High Refractive and Transparent Organic−Inorganic Hybrid Materials. *J. Polym. Sci., Part A: Polym. Chem.* **2011**, *49*, 712−718.

(5) Lee, L. H.; Chen, W. C. High-Refractive-Index Thin Films Prepared from Trialkoxysilane-Capped Poly(Methyl Methacrylate)-Titania Materials. *Chem. Mater.* **2001**, *13*, 1137−1142.

(6) Althues, H.; Henle, J.; Kaskel, S. Functional Inorganic Nanofillers for Transparent Polymers. *Chem. Soc. Rev.* **2007**, *36*, 1454−1465.

(7) Green, P. F. The Structure of Chain End-Grafted Nanoparticle/Homopolymer Nanocomposites. *Soft Matter* **2011**, *7*, 7914−7926.

(8) Gast, A. P.; Leibler, L. Effect of Polymer Solutions on Sterically Stabilized Suspensions. *J. Phys. Chem.* **1985**, *89*, 3947−3949.

(9) Borukhov, I.; Leibler, L. Enthalpic Stabilization of Brush-Coated Particles in a Polymer Melt. *Macromolecules* **2002**, *35*, 5171−5182.

(10) Gast, A. P.; Leibler, L. Interactions of Sterically Stabilized Particles Suspended in a Polymer Solution. *Macromolecules* **1986**, *19*, 686−691.

(11) Lee, S.; Shin, H. J.; Yoon, S. M.; Yi, D. K.; Choi, J. Y.; Paik, U. Refractive Index Engineering of Transparent ZrO_2−Polydimethylsiloxane Nanocomposites. *J. Mater. Chem.* **2008**, *18*, 1751−1755.

(12) Demir, M. M.; Castignolles, P.; Akbey, Ü.; Wegner, G. In-Situ Bulk Polymerization of Dilute Particle/MMA Dispersions. *Macromolecules* **2007**, *40*, 4190−4198.

(13) Zheng, L.; Xie, A. F.; Lean, J. T. Polystyrene Nanoparticles with Anionically Polymerized Polybutadiene Brushes. *Macromolecules* **2004**, *37*, 9954−9962.

(14) Ranjan, R.; Brittain, W. J. Synthesis of High Density Polymer Brushes on Nanoparticles by Combined Raft Polymerization and Click Chemistry. *Macromol. Rapid Commun.* **2008**, *29*, 1104−1110.

(15) Ohno, K.; Morinaga, T.; Koh, K.; Tsujii, Y.; Fukuda, T. Synthesis of Monodisperse Silica Particles Coated with Well-Defined, High-Density Polymer Brushes by Surface-Initiated Atom Transfer Radical Polymerization. *Macromolecules* **2005**, *38*, 2137−2142.

(16) Tao, P.; Viswanath, A.; Li, Y.; Rungta, A.; Benicewicz, B. C.; Siegel, R. W.; Schadler, L. S. Refractive Index Engineering of Polymer Nanocomposites Prepared by End-Grafted Polymer Chains onto Inorganic Nanoparticles. *Mater. Res. Soc. Symp. Proc. U.S.A.* **2011**, *1359*, 163−168.

(17) Meli, L.; Arceo, A.; Green, P. F. Control of the Entropic Interactions and Phase Behavior of Athermal Nanoparticle/Homopolymer Thin Film Mixtures. *Soft Matter* **2009**, *5*, 533−537.

(18) Hasegawa, R.; Aoki, Y.; Doi, M. Optimum Graft Density for Dispersing Particles in Polymer Melts. *Macromolecules* **1996**, *29*, 6656−6662.

(19) Matsen, M. W.; Gardiner, J. M. Autophobic Dewetting of Homopolymer on a Brush and Entropic Attraction between Opposing Brushes in a Homopolymer Matrix. *J. Chem. Phys.* **2001**, *115*, 2794.

(20) Dutta, N.; Green, D. Nanoparticle Stability in Semidilute and Concentrated Polymer Solutions. *Langmuir* **2008**, *24*, 5260−5269.

(21) Ferreira, P. G.; Ajdari, A.; Leibler, L. Scaling Law for Entropic Effects at Interfaces between Grafted Layers and Polymer Melts. *Macromolecules* **1998**, *31*, 3994−4003.

(22) Pryamtisyn, V.; Ganesan, V.; Panagiotopoulos, A. Z.; Liu, H.; Kumar, S. K. Modeling the Anisotropic Self-Assembly of Spherical Polymer-Grafted Nanoparticles. *J. Chem. Phys.* **2009**, *131*, 221102.

(23) Dan, N.; Tirrell, M. Effect of Bimodal Molecular Weight Distribution on the Polymer Brush. *Macromolecules* **1993**, *26*, 6467−6473.

(24) Skvortsov, A.; Gorbunov, A.; Leermakers, F.; Fleer, G. Long Minority Chains in a Polymer Brush: A First-Order Adsorption Transition. *Macromolecules* **1999**, *32*, 2004−2015.
(25) Kent, M.; Factor, B.; Satija, S.; Gallagher, P.; Smith, G. Structure of Bimodal Polymer Brushes in a Good Solvent by Neutron Reflectivity. *Macromolecules* **1996**, *29*, 2843−2849.
(26) Edgecombe, S.; Gardiner, J.; Matsen, M. Suppressing Autophobic Dewetting by Using a Bimodal Brush. *Macromolecules* **2002**, *35*, 6475−6477.
(27) Reiter, G.; Schultz, J.; Auroy, P.; Auvray, L. Improving Adhesion via Connector Polymers to Stabilize Non-Wetting Liquid Films. *Europhys. Lett.* **1996**, *33*, 29.
(28) Zhao, B.; Zhu, L. Mixed Polymer Brush-Grafted Particles: A New Class of Environmentally Responsive Nanostructured Materials. *Macromolecules* **2009**, *42*, 9369−9383.
(29) Sidorenko, A.; Minko, S.; Schenk-Meuser, K.; Duschner, H.; Stamm, M. Switching of Polymer Brushes. *Langmuir* **1999**, *15*, 8349−8355.
(30) Zhao, B. Synthesis of Binary Mixed Homopolymer Brushes by Combining Atom Transfer Radical Polymerization and Nitroxide-Mediated Radical Polymerization. *Polymer* **2003**, *44*, 4079−4083.
(31) Nair, N.; Wentzel, N.; Jayaraman, A. Effect of Bidispersity in Grafted Chain Length on Grafted Chain Conformations and Potential of Mean Force between Polymer Grafted Nanoparticles in a Homopolymer Matrix. *J. Chem. Phys.* **2011**, *134*, 194906.
(32) Norris, A. W.; Bahadur, M.; Yoshitake, M. Novel Silicone Materials for LED Packaging. *Proc. SPIE* **2005**, *5941*, 594115−1.
(33) Tao, P.; Li, Y.; Rungta, A.; Viswanath, A.; Gao, J.; Benicewicz, B. C.; Siegel, R. W.; Schadler, L. S. TiO_2 Nanocomposites with High Refractive Index and Transparency. *J. Mater. Chem.* **2011**, *21*, 18623−18629.
(34) Tao, P.; Viswanath, A.; Schadler, L. S.; Benicewicz, B.; Siegel, R. W. Preparation and Optical Properties of ITO/Epoxy Nanocomposites with Polyglycidyl Methacrylate Grafted Nanoparticles. *ACS Appl. Mater. Interfaces* **2011**, *3*, 3638−3645.
(35) Pan, D.; Zhao, N.; Wang, Q.; Jiang, S.; Ji, X.; An, L. Facile Synthesis and Characterization of Luminescent TiO_2 Nanocrystals. *Adv. Mater.* **2005**, *17*, 1991−1995.
(36) White, M. A.; Johnson, J. A.; Koberstein, J. T.; Turro, N. J. Toward the Syntheses of Universal Ligands for Metal Oxide Surfaces: Controlling Surface Functionality through Click Chemistry. *J. Am. Chem. Soc.* **2006**, *128*, 11356−11357.
(37) Zhang, B.; Kong, T.; Xu, W.; Su, R.; Gao, Y.; Cheng, G. Surface Functionalization of Zinc Oxide by Carboxyalkylphosphonic Acid Self-Assembled Monolayers. *Langmuir* **2010**, *26*, 4514−4522.
(38) Kobayashi, M.; Matsuno, R.; Otsuka, H.; Takahara, A. Precise Surface Structure Control of Inorganic Solid and Metal Oxide Nanoparticles through Surface-Initiated Radical Polymerization. *Sci. Technol. Adv. Mater.* **2006**, *7*, 617−628.
(39) Tchoul, M. N.; Fillery, S. P.; Koerner, H.; Drummy, L. F.; Oyerokun, F. T.; Mirau, P. A.; Durstock, M. F.; Vaia, R. A. Assemblies of Titanium Dioxide-Polystyrene Hybrid Nanoparticles for Dielectric Applications. *Chem. Mater.* **2010**, *22*, 1749−1759.
(40) Akcora, P.; Liu, H.; Kumar, S. K.; Moll, J.; Li, Y.; Benicewicz, B. C.; Schadler, L. S.; Acehan, D.; Panagiotopoulos, A. Z.; Pryamitsyn, V. Anisotropic Self-Assembly of Spherical Polymer-Grafted Nanoparticles. *Nat. Mater.* **2009**, *8*, 354−359.
(41) Lü, C.; Yang, B. High Refractive Index Organic−Inorganic Nanocomposites: Design, Synthesis and Application. *J. Mater. Chem.* **2009**, *19*, 2884−2901.
(42) Hiemenz, P.; Lodge, T. *Polymer Chemistry*, 2nd ed.; CRC Press: Boca Raton, FL, 2007.
(43) Raghavan, S. R.; Hou, J.; Baker, G. L.; Khan, S. A. Colloidal Interactions between Particles with Tethered Nonpolar Chains Dispersed in Polar Media: Direct Correlation between Dynamic Rheology and Interaction Parameters. *Langmuir* **2000**, *16*, 1066−1077.
(44) Israelachvili, J. N. *Intermolecular and Surface Forces*; Academic Press: London, 1992.
(45) Maas, J.; Fleer, G.; Leermakers, F.; Stuart, M. A. C. Wetting of a Polymer Brush by a Chemically Identical Polymer Melt: Phase Diagram and Film Stability. *Langmuir* **2002**, *18*, 8871−8880.
(46) Wijmans, C.; Zhulina, E.; Fleer, G. Effect of Free Polymer on the Structure of a Polymer Brush and Interaction between Two Polymer Brushes. *Macromolecules* **1994**, *27*, 3238−3248.
(47) Cho, S. D.; Lee, S. Y.; Hyun, J. G.; Paik, K. W. Comparison of Theoretical Predictions and Experimental Values of the Dielectric Constant of Epoxy/$BaTiO_3$ Composite Embedded Capacitor Films. *J. Mater. Sci.: Mater. Electron.* **2005**, *16*, 77−84.
(48) Chevigny, C.; Dalmas, F.; Di Cola, E.; Gigmes, D.; Bertin, D.; Boué, F.; Jestin, J. Polymer-Grafted-Nanoparticles Nanocomposites: Dispersion, Grafted Chain Conformation, and Rheological Behavior. *Macromolecules* **2011**, *44*, 122−133.
(49) Sunday, D.; Ilavsky, J.; Green, D. L. A Phase Diagram for Polymer-Grafted Nanoparticles in Homopolymer Matrices. *Macromolecules* **2012**, *45*, 4007−4011.
(50) Tao, P.; Li, Y.; Siegel, R.; Schadler, L. S. Transparent Luminescent Silicone Nanocomposites Filled with Bimodal PDMS-Brush-Grafted CdSe Quantum Dots. *J. Mater. Chem. C* **2013**, DOI: 10.1039/C2TC00057A.